Journal of Non-Crystalline Solids 447 (2016) 29–34

Contents lists available at ScienceDirect

Journal of Non-Crystalline Solids

journal homepage: www.elsevier.com/locate/jnoncrysol

Synthesis of highly destacked ReS_2 layers embedded in amorphous carbon from a metal-organic precursor

Juan Antonio Aliaga [a,b,*], Gabriel Alonso-Núñez [c,e], Trino Zepeda [c], Juan Francisco Araya [a,f], Pedro Felipe Rubio [a], Zaira Bedolla-Valdez [c], Francisco Paraguay-Delgado [d], Mario Farías [c], Sergio Fuentes [c], Guillermo González [a,g]

[a] Laboratorio de Química Inorgánica y Electroquímica, Departamento de Química, Facultad de Ciencias, Universidad de Chile, Las Palmeras, 3425 Ñuñoa, Santiago, Chile
[b] Departamento de Química, Universidad Tecnológica Metropolitana, José Pedro Alessandri, 1242 Ñuñoa, Santiago, Chile
[c] Centro de Nanociencias y Nanotecnología, Universidad Nacional Autónoma de México, Ensenada, Baja California C.P. 22860, Mexico
[d] Centro de investigación en materiales avanzados, CIMAV, Miguel de Cervantes 120, C.P. 31136, Chihuahua, Mexico
[e] Institut de Recherches sur la Catalyse et l'Environnement, IRCELYON, CNR, University of Lyon, Villeurbanne 69100, France
[f] Departamento de Geología, Universidad de Atacama, Copayapu 485, Copiapó, Chile
[g] Center for the Development of Nanocience and Nanotechnology, CEDENNA, Santiago, Chile

ARTICLE INFO

Article history:
Received 14 February 2016
Received in revised form 12 May 2016
Accepted 14 May 2016
Available online 24 May 2016

Keywords:
Amorphous materials
Nanostructured materials
Chemical synthesis
Rhenium disulfide
Hydrothermal synthesis

ABSTRACT

In the current study, a new approach to the synthesis of highly destacked ReS_2 layers embedded in amorphous carbon via the thermal decomposition of a tetraoctylammonium perrhenate precursor, under sulfidizing atmosphere (15% v/v H_2S mixture H_2S/H_2 gas), is described. X-ray diffraction, scanning electron microscopy, scanning transmission electron microscopy, energy-dispersive X-ray spectroscopy and X-ray photoelectron spectroscopy analysis of the thermolysis product confirm the formation of rhenium disulfide. The synthesized compound is found as single layers with a minor proportion of few-layer arrangements, embedded in amorphous carbon. X-ray diffraction, UV–visible diffuse reflectance, and thermogravimetry analysis were made in order to characterize the metal-organic salt precursor, showing that the perrhenate ions are dispersed widely from each other in the matrix of the organic cations, forming an inorganic-organic salt. The special arrangement of these ReS_2 layers has a potential use as a heterogeneous catalyst due to the high proportion of edge sites.

1. Introduction

Rhenium disulfide (ReS_2) is a transition metal dichalcogenide (TMDC), composed of S-Re-S 2D layers stacked and held together perpendicularly to the layer plane by van der Waals forces [1]. One of the most remarkable characteristics of the solid ReS_2 is the low interaction energy between layers and the direct band gap value near to that of a single layer [2,3]. The typical high anisotropy of this layered compound in particular is further increased by the unique feature of presenting an intralayer Re—Re bond, and improving in-plane anisotropic transport and optical properties to thin 2D layered ReS_2 materials [4]. Even when this is one of the least studied TMDC's, ReS_2 has recently called the attention because the vibrational and optical properties of their bulk behaves like individual monolayers, which strongly contrast with the properties of other TMDCs like MoS_2 and WS_2 [2,5]. The chemistry of ReS_2 is still incipient, however it has been used as a catalyst in hydrotreating reactions [6], as an electrocatalyst in hydrogen evolution reactions [7], in radiation synovectomy [8], in field effect transistors [9] and in high current density lithium ion batteries [10]. Until now, various ReS_2 structures have been attained in a relatively controllable way by methods of solid-state and soft chemistry using an appropriate selection of precursors, solvent, additives and/or reaction conditions [11–13].

Poorly-crystalline TMDC-based nanostructured products with high surface area have been obtained using the strategy proposed by Alonso et al. [14,15] using tetraalkylammonium thiometallates (M = Mo or W) as a source of both metal and carbon. In these compounds the stacking along the c-axis of the sulfide layers is prevented in a certain grade by the carbon component, leading to more amorphous materials. Concerning rhenium sulfide in particular, as far as we know, there is only one report dealing with the synthesis of rhenium disulfide using tetraethylammonium thioperrhenate as a precursor $(Et_4N)ReS_4$; however the structural characterization of the product and possible effects of the carbon component involved in the synthesis were not reported at the time [16]. Herein, we present a facile new approach for the synthesis of ReS_2/C nanocomposites by direct sulfidization (H_2S/H_2) of a bulky perrhenate metal-organic salt $(Oct_4N)ReO_4$; the isolation of the perrhenate ions in the organic cation matrix modulates the sulfidizing

* Corresponding author at: Laboratorio de Química Inorgánica y Electroquímica, Departamento de Química, Facultad de Ciencias, Universidad de Chile, Las Palmeras, 3425 Ñuñoa, Santiago, Chile.
E-mail address: jaliaga@utem.cl (J.A. Aliaga).

http://dx.doi.org/10.1016/j.jnoncrysol.2016.05.033
0022-3093/

reaction, leading to rhenium sulfide layers embedded in a carbonaceous medium with small sizes and high exposure of the edges sites.

2. Experimental details

2.1. Preparation of ReS_2/C

Ammonium perrhenate NH_4ReO_4 (6.0 mmol) was dissolved in water (30 ml), and this solution was added to 6.0 mmol of tetra-*n*-octylammonium bromide $(Oct_4N)Br$ which was previously dissolved in a solution of 10 ml of water and 5 ml of ethanol at 70 °C. A white precipitate was immediately formed by an ionic exchange reaction; this white powder was washed with distilled water and let dry at room temperature. To obtain the rhenium sulfide monolayers, the precursor was decomposed under a reductive atmosphere: $(Oct_4N)ReO_4$ was placed in a tubular reactor, heated up to 400 °C at 2 °C/min under a flow of H_2S (15%) in hydrogen gas, and kept under these conditions for 4 h. The sample was then cooled down naturally at room temperature.

2.2. Materials characterization

X-ray diffraction patterns (XRD) were obtained by a Philips X'pert MPD powder diffractometer operating at 30 mA and 40 kV, using CuKα radiation (k = 1.54060 Å). Scanning electron microscopy (SEM) images were taken in a JEOL JIB 4500 electron microscope operated at 15 kV. Scanning transmission electron microscopy (STEM) and energy-dispersive X-ray spectroscopy (EDS) were conducted using a JEOL 2000FS operating at 200 kV. Differential thermal gravimetry (DTG) and thermal gravimetry (TG) measurements were carried out on Q600 TA instrument; the sample was heated under a helium atmosphere at a rate of 10 °C/min to 800 °C. UV–vis diffuse reflectance spectra (DR) were recorded by a CARY 300 SCAN VARIAN spectrophotometer. X-ray photoelectron spectra (XPS) of sulfide catalysts were carried out in a SPECS GmbH custom made system using a PHOIBOS 150 WAL hemispherical analyzer and a μ-FOCUS 500 X-ray source. All data was acquired using monochromated AlKα X-rays (1486.6 eV, 110 W), pass energy of 50 eV and high-intensity lens mode. The diameter of the area analyzed was 0.88 mm. The pressure in the analysis chamber was maintained lower than 2×10^{-9} mbars. Sulfide catalysts were mounted on a sample holder and kept overnight in high vacuum in the preparation chamber before they were transferred to the analysis chamber of the spectrometer. Charge referencing was done against adventitious carbon (C 1s 284.5 eV). Energy regions for C 1s, O 1s, S 2p and Re 4f were selected and scanned 20 times, with a dwell time of 0.2 s and an energy step of 0.1 eV. Spectra are presented with intensity in counts-per-second (CPS) without smoothing and a Shirley-type background was subtracted. Fits of the experimental peaks were obtained using combinations of Gaussian/Lorentzian lines with a 70/30 proportion using Casa XPS from Casa Software Ltd. The peaks binding energy and FWHM were allowed to vary, although the same width was kept among all lines. Single peaks were utilized for C 1s and O 1s transitions. Spin-orbit splitting ratios of 2:1 for the sulfur $2p_{3/2}$ to $2p_{1/2}$ and 4:3 for rhenium $4f_{7/2}$ to $4f_{5/2}$ doublets, with the corresponding separation in binding energy of 1.18 eV and 2.43 eV were implemented. Relative atomic concentrations were calculated considering peak areas and atomic sensitivity factors from a Handbook [17]. The accuracy of the binding energy values is ±0.1 eV.

After fitting, the values obtained for the standard deviation from comparing the experimental data towards the envelope (sum of doublet lines) from fitting the Re4f energy region and the corresponding adjusted R-square values were 6.43 and 0.99936, respectively. Also, the standard deviation area (SDA) values between the experimental data and the sum of areas of fitting doublet lines were compared to experimental data areas (A) and that the obtained SDA/A ratio for Re 4f was 0.014.

3. Results

3.1. XRD analysis

The XRD pattern of the product as-prepared by the thermal decomposition of $(Oct_4N)ReO_4$ under H_2S/H_2 atmosphere is shown in Fig. 1. The diffractogram shows two broad low-intensity diffraction peaks centered on 2θ = 33° and 44°, which can be indexed as the Bragg reflections (200) and (006) of layered ReS_2 (JCPDS 89-0341). The shape of the diffractogram is the typical one of a poorly-crystalline ReS_2 phase [18]. The conspicuous absence of the (002) peak at 2θ = 14.5° points out an extremely low stacking degree along the crystallographic c-axis of the ReS_2, characteristic of monolayered structures [19].

3.2. Morphology and composition

The morphology of the product was examined by scanning electron microscopy (SEM) and scanning transmission electron microscopy (STEM). The sample is composed by microscopic irregular grains (Fig. 2a), with diameters between 0.1 and 2.0 μm. However, a closer analysis shows that the grains appear to be formed by agglomeration of submicrometric platelets. The STEM images of the product reveal a higher proportion of poorly stacked nanosheets with random orientation (Fig. 2b). In Figs. 2b–c we can detect a few thin arrangements of some stacked layers along the c-axis with an average interplanar distance of 0.62 nm. The latter is corroborated by the diffuse diffraction rings observed in the corresponding selected area electron diffraction (SAED) patterns (inset Fig. 2b). A quantitative layer length was obtained through statistical analysis based on 400 layers taken from different parts of the STEM images; the longitudinal slab length of the layers account in average approximately 4.81 nm ± 1.52 nm in length (Fig. 2d). An estimation of the composition of the product was attempted by energy-dispersive X-ray spectroscopy (EDS). As observed in Fig. S1, the sample contains rhenium, sulfur, and carbon; however a significant amount of oxygen is also detected. The analysis reveals a S:Re ratio of about 1:1.55, and carbon and oxygen contents of about 35.2% and 31.4% at. respectively.

The composition of the product was also investigated by X-ray photoelectron spectroscopy. The spectra in Figs. 3a and 3b corroborate the presence of ReS_2 in the sample. Fig. 3 and Fig. S2 shows the XPS spectra in the regions of rhenium, sulfur and carbon. Indeed, peaks at 41.9 ± 0.1 eV (Fig. 3a) and 162.7 ± 0.1 eV (Fig. 2Sa) that are respectively characteristic for Re $4f_{4/7}$ and S $2p_{3/2}$ electrons in the ReS_2 are clearly observed [20,21]. However, the rhenium spectrum (Fig. 3a) also reveals the presence of other photogenerated Re f electrons with higher relative binding energies. The deconvolution of three additional doublets on the rhenium curve (Fig. 3a) indicate the presence of oxides on the surface of

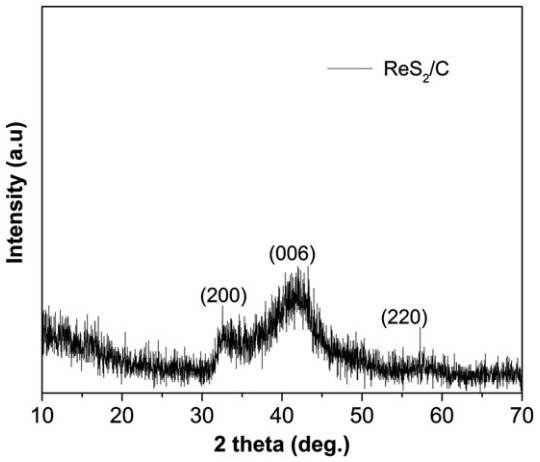

Fig 1. Powder XRD patterns of obtained ReS_2/C.

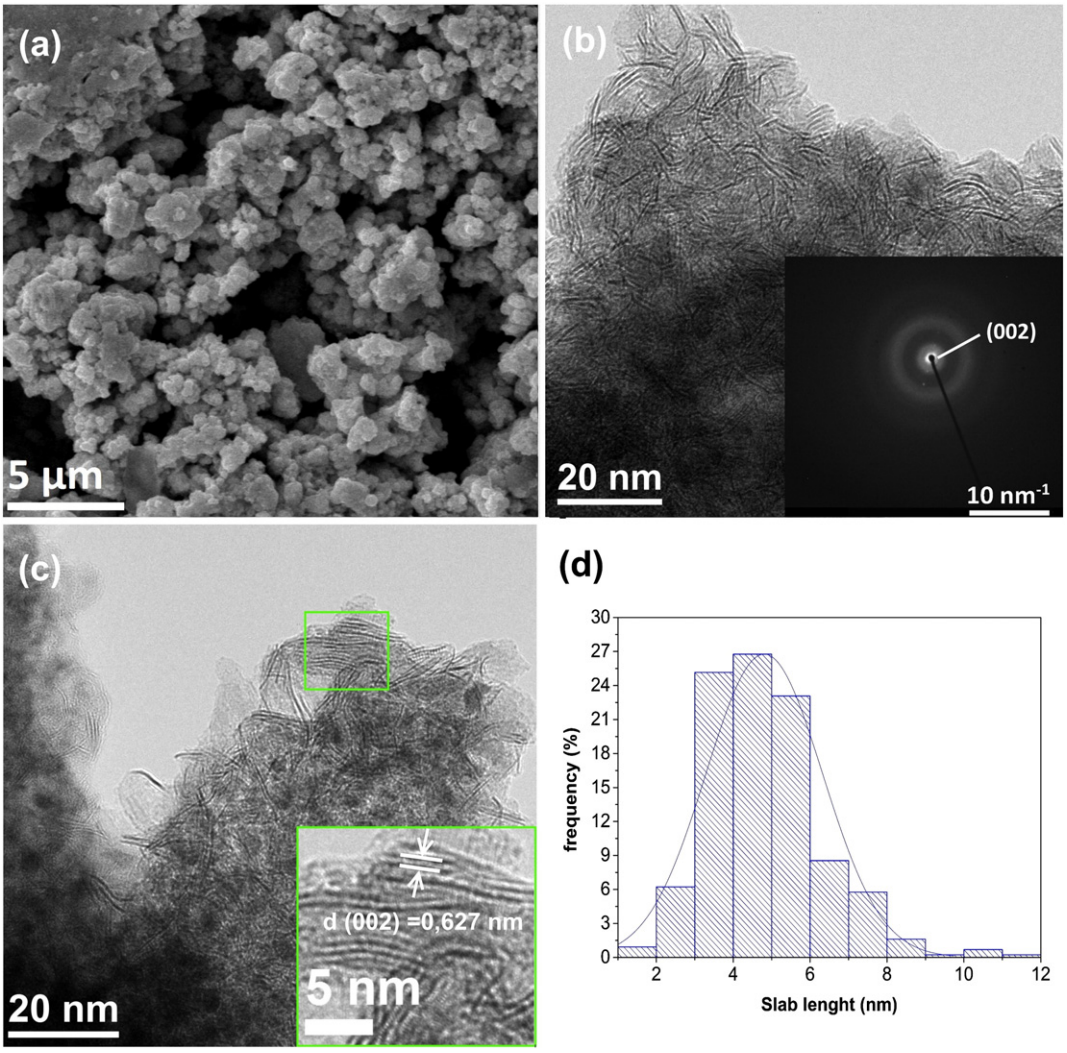

Fig 2. SEM image (a) and STEM images of ReS_2/C (b)–(d).

the sample; traces of ReO_2 (43.5 ± 0.1 eV), ReO_3 (45.7 ± 0.1 eV) and Re_2O_7 (46.6 ± 0.1 eV) respectively for Re $4f_{4/7}$ [22,23]. Moreover in the sulfur spectrum (Fig. S2a) an emission attributable to sulfate is also apparent (169.2 ± 0.1 eV). The spectrum of carbon (Fig. S2b) shows in turn the typical shape of carbonaceous materials where emissions assignable to several organic groups, aromatic C═C (284 ± 0.1 eV), aliphatic C—C(285 ± 0.1 eV) and hydroxyl carbon C—O (286.1 ± 0.1 eV) can be identified [24].

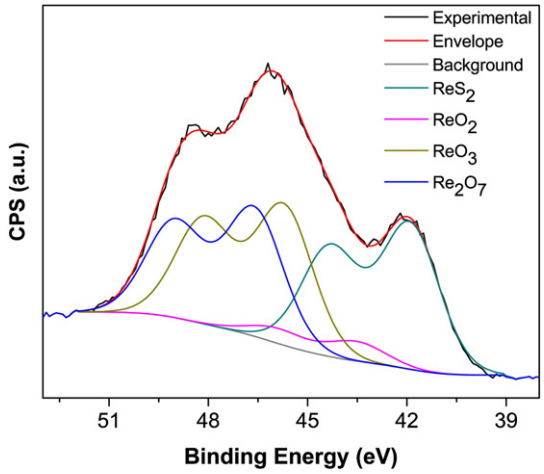

Fig 3. XPS spectra of the Re 4f core electron levels of ReS_2/C.

3.3. Spectroscopic and thermal study of the precursor

The peculiar arrangement of ReS_2 nanosheets communicated in this paper is clearly determined by the nature of the rhenium precursor used in the synthesis. In order to rationalize our results, a more detailed study of the $(Oct_4N)ReO_4$ was undertaken. The Fig. 4(a) shows the diffuse reflectance spectra of NH_4ReO_4 and $(Oct_4N)ReO_4$; ammonium perrhenate is used as reference, showing a single absorption band at ~275 nm, product of the ReO_4^- units, while that of the octylammonium derivative is centered at 251 nm. This high energy shift is indicative of isolated and distorted ReO_4^- units [25].

Fig. 4(b) shows the TGA–DTG curves of the precursor $(Oct_4N)ReO_4$: the 2% weight loss in the range of 190°–260° corresponds to the evaporation of water and other volatile impurities trapped in the material. The second and most important weight loss of 64.9% (theoretical 65.1 wt%) observed in the range of 270°–370° is assigned to the thermal decomposition of tetraoctylammonium. The single-step decomposition of the tetraoctylammonium cation agrees with results reported by Alonso et al. [14], while the weight loss in the range 350–450 °C may correspond to the volatilization of a small amount of Re_2O_7, arising from the thermal dehydration of perrhenic acid generated by the presence of water and

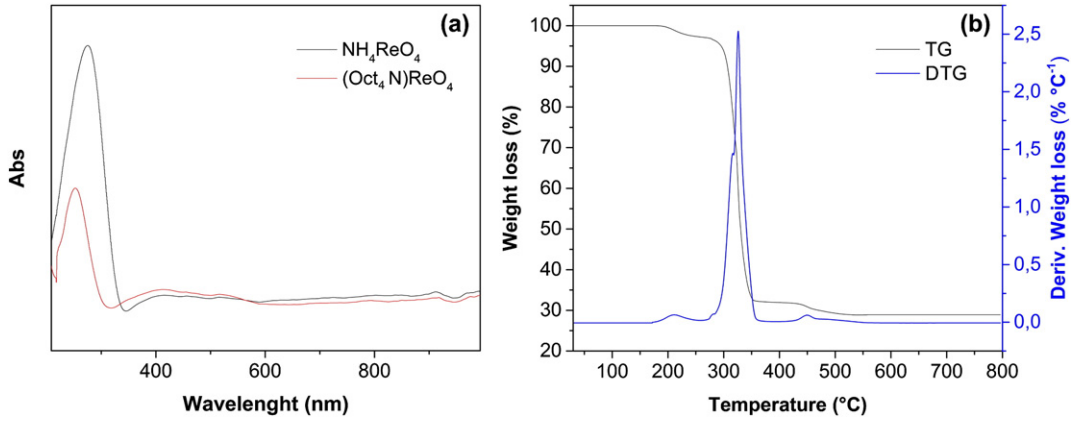

Fig 4. (a) UV–vis diffuse reflectance spectra of $(Oct_4N)ReO_4$ and NH_4ReO_4 and (b) TGA–DTG curves of the $(Oct_4N)ReO_4$.

by the concomitant formation of ReO_3 species. The remaining solid corresponds to residual ReO_2 [26].

3.4. XRD analysis of the precursor

Fig. 5 shows the XRD pattern of ammonium perrhenate (Fig. 5a) and of synthesized tetraoctylammonium perrhenate (Fig. 5b). Diffractograms indicate that $(Oct_4N)ReO_4$ crystallizes in a scheelite-like structure similar to that of the NH_4ReO_4 reported by Swaison et al. [27], but much more expanded, due to the large size of the tetraoctylammonium cation. All diffraction peaks (Fig. 5b) can be indexed as a pure tetragonal structure with a space group of $I41/a$, with unit cell parameters a = b = 17.971 Å and c = 37.337 Å ($\alpha = \beta = \gamma = 90$). The lattice sample parameters were obtained with the general lattice analysis system program CHECKCELL. Although both perrhenate salts, the ammonium and the tetraoctylammonium ones have similar crystallographic structures; in the latter, the connectivity among perrhenate species results rather peculiar. In the scheme of Fig. 6 the structure of the metal organic salt is represented showing the preferential (011) plane in the proposed reaction.

4. Discussion

Strategies leading to the synthesis of TMDC-based catalysts, avoiding crystallization extensive processes are in general important in order to enhance the concentration of active sites [28]. The catalyst dispersion in carbon matrices has proved to be a valuable approach for preparing numerous products based on sulfides of molybdenum [14] or rhenium sulfides [29]. The aim of this work was to produce ReS_2/carbon composites with high proportion of edges sites using the carbon-rich rhenium-precursor tetraoctylammonium perrhenate, $(Oct_4N)ReO_4$.

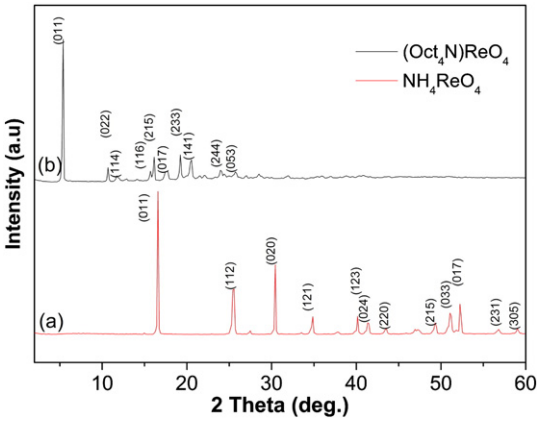

Fig 5. (a) XRD patterns of (a) NH_4ReO_4 and (b) $(Oct_4N)ReO_4$.

The direct reductive sulfidization of solid tetraoctylammonium perrhenate with the gaseous mixture 15% H_2S in H_2 at 400 °C leads to the formation of ReS_2 and carbonaceous matter. The XRD pattern of the product indicates that the ReS_2 is formed in a highly amorphous state; as expected for these materials, the two Bragg reflections at $2\theta = 33°$ and 44°, characteristic for layered ReS_2, are observed as broad, low-intensity peaks [18]. However, it results rather remarkable that none of the typical low-angle (00*l*) reflections, typical of layered TMDC, are observed. Thus, this points to a product where the layer stacking is highly inhibited. This feature was corroborated by the electron microscopy analysis of the sample; indeed, STEM images show that the sample contains highly disordered and bent ReS_2 nanosheets. Most of the rhenium disulfide is represented by single layers, with a minor proportion of a few-layer arrangements, where the layers are stacked with a *d*-spacing (*d*002) of 0.62 nm, in agreement with the *d*-spacing for crystalline ReS_2 (JCPDS 89–0341). This also agrees with SAED measurements leading to a diffuse (002) ring.

The XPS analysis of the sample corroborated the formation of ReS_2. Additionally, these spectra revealed that the sample also contains rhenium oxides, namely ReO_2, ReO_3 and Re_2O_7 (by the deconvolution of three additional doublets), as well as carbonaceous matter. This agrees with the composition of the sample estimated by EDS. Since XRD data does not show any reflection assignable to these oxides, they may be found as amorphous phases, either dispersed in the bulk or adsorbed within the ReS_2-carbonaceous composite.

In both cases the formation of oxide phases may be explained by considering some particularities of the synthesis method used for producing this composite. We can distinguish two processes involving the formation of oxides. On one side, a surface process associated with the sulfidization of the rhenium precursor by using hydrogen in the sulfidizing mixture (H_2S/H_2) implies the formation of low-valence rhenium species, as well as of sulfur-deficient ReS_{2-x} [23]. These metastable, highly reactive intermediates are very susceptible to oxidation, so that they could react with air to produce stable rhenium oxides at sample surface while manipulation. On the other side, the presence of oxides in the bulk could arise from an incomplete sulfidization process due to a shielding phenomenon [30]. Independently of complexities inherent to the solid-gas reaction used here — among them the formation of rhenium oxidized species already discussed — the morphology of the as-synthesized ReS_2 deserves further attention. The known trend of ReS_2 to produce disordered phases with low stacking degree is expected to further increase the disorder when inserted in a carbonaceous matrix. However, to the best of our knowledge, the preparation of ReS_2 solid phases with a destacking degree like the one described here has not been reported until now, even in other preparations of ReS_2/C nanocomposites [16,31]. Therefore, we propose that the high dispersion of

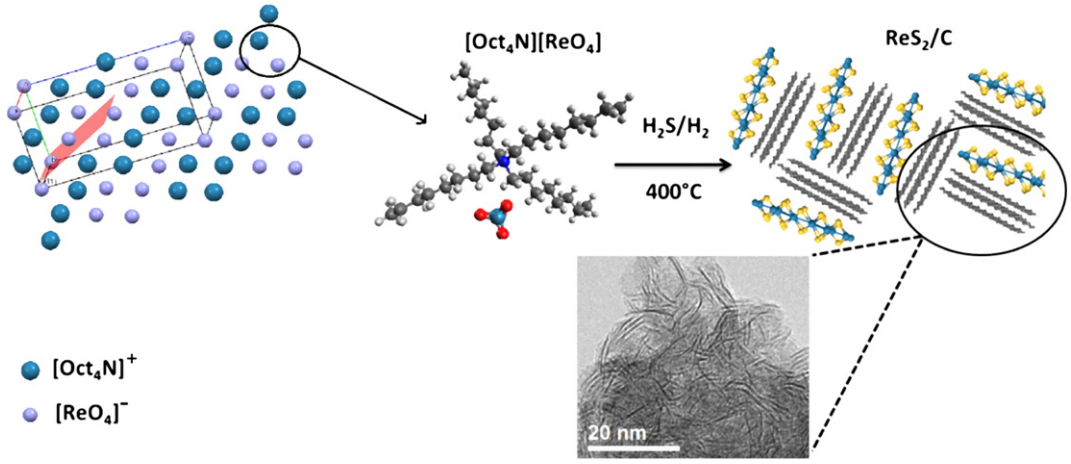

Fig 6. Illustration of the formation of ReS_2/C dispersed layers prepared by thermal decomposition of metal-organic precursor.

the sulfide layers is a consequence of the nature of the precursor $(Oct_4N)ReO_4$; particularly due to its alkylic component, which leads to the concomitantly formation of carbonaceous matter during the thermal decomposition. In that direction we undertake a somewhat more detailed study of the precursor $(Oct_4N)ReO_4$. Hypothesizing that the peculiar effect of this salt on ReS_2 morphology (destacked small layers) is mainly due to the voluminous tetraalkylammonium cation, we centered our attention in the structure, stability, and interactions of $(Oct_4N)ReO_4$ in the solid state in comparison with those of the $(NH_4)ReO_4$.

The diffraction pattern of the $(Oct_4N)ReO_4$ can be indexed as a Scheelite-like structure, similar to that reported for the NH_4ReO_4 in the literature [32]. In spite of the similitude of both structures, the expansion caused by the volume of the tetralkylammonium cation changes significantly the connectivity among the perrhenate anions. Contrasting with the NH_4ReO_4 where the distance between two perrhenate ions is 5.36 Å, in the metal organic salt these ions are much more distant from each other 16.38 Å along the (011) plane (Fig. S3). In both compounds the high energy shift is in agreement with the XRD patterns and they indicate isolated anions due to the spacing effect of the tetralkylammonium cation. ReO_4^- anions are enough apart restricting the diffusion during the reaction. The role of $(Oct_4N)ReO_4$ in modulating the morphology of obtained ReS_2/C composite may be rationalized at the light of the properties of the precursor already commented. We assume that the mechanism of sulfidization of this precursor is similar to that of the NH_4ReO_4 [28]; i.e. an initial condensation of ReO_4^- units to produce Re_2O_7 clusters followed by their reaction with H_2S for generating the ReS_2 layers. Consequently, the growth of products, intermediary and final, is expected to be mainly modulated by the mobility of the ReO_4^- ions in the precursor.

This synthesis strategy resembles the use of ionic liquids to synthesize inorganic nanomaterials with special morphological properties; for example in the preparation of ZnSe hollow nanospheres using a quaternary ammonium liquid ionic [32]. However, it differs in that the reaction described here occurs in a solid state. Moreover, though tetraalkylammonium salts have been used for designing ionic liquid analogues, these salts are not themselves liquid ionic. Therefore, we suggest that the mobility of the ReO_4^- ions, required for their condensation into Re_2O_7 crystallites arises from the behavior of the $Octil_4N$ as ionic plastic crystal. The short-range structural disorder in these materials typically associated with rotational and/or configuration changes of the ions, enhances ion mobility beyond the steric hindrances and electrostatic interactions common in normal ionic compounds. These effects should gradually increase with increasing temperature until the precursor decomposes to produce carbonaceous materials.

Thus, the high confinement degree of the perrhenate anions in the $(Oct_4N)ReO_4$ demonstrated above, together with the ionic plastic crystal nature of this salt, explains satisfactorily the small size of the ReS_2/C particles observed. Additionally, the concomitant formation of carbonaceous material by thermal decomposition of the metal-organic precursor, would further limit the agglomeration Re_2O_7-crystallite as well as the stacking of ReS_2 sheets.

5. Conclusions

Highly destacked ReS_2 layers dispersed in amorphous carbon were successfully obtained from the decomposition of $(Oct_4N)ReO_4$ at 400 °C, sulfidized under a reductive atmosphere. $(Oct_4N)ReO_4$ was previously synthesized via an anionic exchange reaction of $(Oct_4N)Br$ and NH_4ReO_4. The ReS_2/C product consists in randomly orientated and poorly stacked layers of rhenium disulfide — with a large proportion of edge sites — embedded in amorphous carbon. The sample contained about 35 at.% of amorphous carbon, derived from the decomposition of the tetraoctylammonium cation; this carbonaceous matter hinders the further stacking between the rhenium sulfide layers and its growth. The special arrangement of these ReS_2 layers has a potential use in hydrodesulfurization catalysts and opens the path to the preparation of new rhenium complexes by changing the size of the alkylammonium group, in comparatively mild-energy solvothermal synthesis processes.

Acknowledgements

The authors thank FONDECYT Grant 1131112, CONICYT FB0807 (CEDENNA), CONACYT (174689, 155388), PAPIIT (IN104714-3), CONICYT 21120311 Doctoral Fellowship (Juan Aliaga), CONACYT (sabbatical 259931) and to W. Antúnez and C. Ornelas for their technical help. We are very grateful to David A. Domínguez for his valuable technical support obtaining the XPS spectra. We are also thankful to the anonymous reviewers whose corrections improved our manuscript.

Appendix A. Supplementary data

Supplementary data to this article can be found online at http://dx.doi.org/10.1016/j.jnoncrysol.2016.05.033.

References

[1] H.-J. Lamfers, A. Meetsma, G. Wiegers, J. De Boer, The crystal structure of some rhenium and technetium dichalcogenides, J. Alloys Compd. 241 (1996) 34–39.
[2] S. Tongay, H. Sahin, C. Ko, A. Luce, W. Fan, K. Liu, J. Zhou, Y.-S. Huang, C.-H. Ho, J. Yan, Monolayer behaviour in bulk ReS_2 due to electronic and vibrational decoupling, Nat. Commun. 5 (2014).
[3] K. Xu, H.-X. Deng, Z. Wang, Y. Huang, F. Wang, S.-S. Li, J.-W. Luo, J. He, Sulfur vacancy activated field effect transistors based on ReS_2 nanosheets, Nanoscale 7 (2015) 15757–15762.

[4] D.A. Chenet, O.B. Aslan, P.Y. Huang, C. Fan, A.M. van der Zande, T.F. Heinz, J.C. Hone, In-plane anisotropy in mono- and few-layer ReS_2 probed by Raman spectroscopy and scanning transmission electron microscopy, Nano Lett. 15 (2015) 5667–5672.
[5] L. Hart, S. Dale, S. Hoye, J.L. Webb, D. Wolverson, Rhenium dichalcogenides: layered semiconductors with two vertical orientations, Nano Lett. 16 (2016) 1381–1386.
[6] N. Escalona, M. Vrinat, D. Laurenti, F. Gil Llambías, Rhenium sulfide in hydrotreating, Appl. Catal. A Gen. 322 (2007) 113–120.
[7] T. Fujita, Y. Ito, Y. Tan, H. Yamaguchi, D. Hojo, A. Hirata, D. Voiry, M. Chhowalla, M. Chen, Chemically exfoliated ReS_2 nanosheets, Nanoscale 6 (2014) 12458–12462.
[8] Y. Junfeng, Z. Ruping, D. Xinlan, M. Xiaofeng, X. Jianying, H. Weiqing, Y. Duanzhi, Z. Wei, X. Hong, W. Yongxian, Intratumoral injection with [^{188}Re] rhenium sulfide suspension for treatment of transplanted human liver carcinoma in nude mice, Nucl. Med. Biol. 27 (2000) 347–352.
[9] E. Liu, Y. Fu, Y. Wang, Y. Feng, H. Liu, X. Wan, W. Zhou, B. Wang, L. Shao, C.-H. Ho, Integrated digital inverters based on two-dimensional anisotropic ReS_2 field-effect transistors, Nat. Commun. 6 (2015).
[10] Q. Zhang, S. Tan, R.G. Mendes, Z. Sun, Y. Chen, X. Kong, Y. Xue, M.H. Rümmeli, X. Wu, S. Chen, Extremely weak van der Waals coupling in vertical ReS_2 nanowalls for high-current-density lithium-ion batteries, Adv. Mater. 28 (2016) 2616–2623.
[11] K. Keyshar, Y. Gong, G. Ye, G. Brunetto, W. Zhou, D.P. Cole, K. Hackenberg, Y. He, L. Machado, M. Kabbani, Chemical vapor deposition of monolayer rhenium disulfide (ReS_2), Adv. Mater. 27 (2015) 4640–4648.
[12] J.A. Aliaga, J.F. Araya, H. Lozano, E. Benavente, G. Alonso-Nuñez, G. González, An easy one-pot solvothermal synthesis of poorly crystalline solid ReS_2/C microspheres, Mater. Chem. Phys. 151 (2014) 372–377.
[13] J.A. Aliaga, J.F. Araya, R. Villarroel, H. Lozano, G. Alonso-Nuñez, G. González, Rhenium and molybdenum poorly crystalline disulfides and their mesophases with hexadecylamine, J. Coord. Chem. 67 (2014) 3884–3893.
[14] G. Alonso, G. Berhault, A. Aguilar, V. Collins, C. Ornelas, S. Fuentes, R. Chianelli, Characterization and HDS activity of mesoporous MoS_2 catalysts prepared by in situ activation of tetraalkylammonium thiomolybdates, J. Catal. 208 (2002) 359–369.
[15] G. Alonso, G. Berhault, F. Paraguay, E. Rivera, S. Fuentes, R.R. Chianelli, Mesoporous carbon-containing MoS_2 materials formed from the in situ decomposition of tetraalkylammonium thiomolybdates, Mater. Res. Bull. 38 (2003) 1045–1055.
[16] C.J. Jacobsen, E. Törnqvist, H. Topsøe, HDS, HDN and HYD activities and temperature-programmed reduction of unsupported transition metal sulfides, Catal. Lett. 63 (1999) 179–183.
[17] J.F. Moulder, J. Chastain, R.C. King, Handbook of X-ray Photoelectron Spectroscopy: A Reference Book of Standard Spectra for Identification and Interpretation of XPS Data, Physical Electronics Eden Prairie, MN, 1995.
[18] W. Tu, B. Denizot, Synthesis of small-sized rhenium sulfide colloidal nanoparticles, J. Colloid Interface Sci. 310 (2007) 167–170.
[19] Y. Peng, Z. Meng, C. Zhong, J. Lu, W. Yu, Y. Jia, Y. Qian, Hydrothermal synthesis and characterization of single-molecular-layer MoS_2 and $MoSe_2$, Chem. Lett. (2001) 772–773.
[20] D. Laurenti, K. Thi, N. Escalona, L. Massin, M. Vrinat, F. Llambías, Support effect with rhenium sulfide catalysts, Catal. Today 130 (2008) 50–55.
[21] C. Sepulveda, R. Garcia, N. Escalona, D. Laurenti, L. Massin, M. Vrinat, Unexpected support effect in hydrotreating: evidence of a metallic character for ReS_2/Al_2O_3 and ReS_2/SiO_2 catalysts, Catal. Lett. 141 (2011) 987–995.
[22] S. Oktay, Z. Kahraman, M. Urgen, K. Kazmanli, XPS investigations of tribolayers formed on TiN and (Ti,Re)N coatings, Appl. Surf. Sci. 328 (2015) 255–261.
[23] J. Okal, A study of effect of particle size on the oxidation of rhenium in the Re/γ-Al_2O_3 catalysts, Appl. Catal. A Gen. 287 (2005) 214–220.
[24] H.-W. Tien, Y.-L. Huang, S.-Y. Yang, J.-Y. Wang, C.-C.M. Ma, The production of graphene nanosheets decorated with silver nanoparticles for use in transparent, conductive films, Carbon 49 (2011) 1550–1560.
[25] N. Escalona, J. Ojeda, R. Cid, G. Alves, A.L. Agudo, J.G. Fierro, F.G. Llambıas, Characterization and reactivity of Re(x)/γ-Al_2O_3 catalysts in hydrodesulfurization and hydrodenitrogenation of gas oil: effect of Re loading, Appl. Catal. A Gen. 234 (2002) 45–54.
[26] B. Meng, Z.-h. Liu, L.-j. Zhou, Z.-y. Liu, C.-f. Zhang, Preparation of ultrafine rhenium powders by CVD hydrogen reduction of volatile rhenium oxides, Trans. Nonferrous Metals Soc. China 23 (2013) 538–542.
[27] I. Swainson, R. Brown, Refinement of ammonium perrhenate structure using a pseudo-spin model for the ammonium ion orientation, Acta Crystallogr. Sect. B: Struct. Sci. 53 (1997) 76–81.
[28] T.F. Jaramillo, K.P. Jørgensen, J. Bonde, J.H. Nielsen, S. Horch, I. Chorkendorff, Identification of active edge sites for electrochemical H_2 evolution from MoS_2 nanocatalysts, Science 317 (2007) 100–102.
[29] N. Escalona, M. Yates, P. Ávila, A.L. Agudo, J. Garcí, J. Ojeda, F. Gil-Llambí, Effect of Re loading on the structure, activity and selectivity of Re/C catalysts in hydrodenitrogenation and hydrodesulphurisation of gas oil, Appl. Catal. A Gen. 240 (2003) 151–160.
[30] K.S. Coleman, J. Sloan, N.A. Hanson, G. Brown, G.P. Clancy, M. Terrones, H. Terrones, M.L. Green, The formation of ReS_2 inorganic fullerene-like structures containing Re_4 parallelogram units and metal—metal bonds, J. Am. Chem. Soc. 124 (2002) 11580–11581.
[31] T. Ho, Q. Shen, J. McConnachie, C. Kliewer, Kinetic characterization of unsupported ReS_2 as hydroprocessing catalyst, J. Catal. 276 (2010) 114–122.
[32] X. Liu, J. Ma, P. Peng, W. Zheng, One-pot hydrothermal synthesis of ZnSe hollow nanospheres from an ionic liquid precursor, Langmuir 26 (2010) 9968–9973.